RSC Advances

PAPER

View Article Online
View Journal | View Issue

Cite this: *RSC Adv.*, 2025, **15**, 50010

A study of stable half-metallic variant perovskites X_2TaCl_6 (X = K, Cs) for possible spintronic applications

Malak Azmat Ali *[a] and Omar Alsalmi[b]

In this study, we present first-principles calculations of the X_2TaCl_6 (X = K, Cs) compounds, which are cubic, perovskite-related inorganic materials analogous to K_2PtCl_6-type structures. The computations were performed using the full-potential linearized augmented plane wave method implemented in the Wien2k code. Exchange–correlation effects were treated within the generalized gradient approximation, with and without the inclusion of a Hubbard parameter to account for electronic correlations. Dynamical stability was confirmed through positive phonon frequencies. The relative stability of ferromagnetic and antiferromagnetic phases was assessed *via* volume optimization, revealing ferromagnetic ground states for both compounds. Structural parameters, including lattice constants, bulk modulus, pressure dependence of the bulk modulus, volume, and ground state energies, were computed and compared with available experimental and theoretical data. Electronic structure analysis indicated a half-metallic behavior in both compounds, with each exhibiting a total magnetic moment of 1μ_B. The Curie temperatures, estimated using the random phase approximation, were found to be 583.55 K for K_2TaCl_6 and 612.30 K for Cs_2TaCl_6. These findings suggest that both variants perovskites, X_2TaCl_6 are promising candidates for spintronic applications.

Received 4th October 2025
Accepted 9th December 2025

DOI: 10.1039/d5ra07551c

rsc.li/rsc-advances

1 Introduction

The term "spintronics" is derived from the French portmanteau for "spin transport electronics." Currently, spintronics is considered a separate branch of physics that focuses on memory, logic, artificial synapses, and the management, storage and transfer of data *via* the spin of electrons.[1] Spintronics differs from conventional electronics in that it utilizes both charge and the spin channels of electrons as degrees of freedom to enhance data efficiency and storage transfer.[2] For applications based on spintronics, there is a need for materials that exhibit high storage density, low power consumption, high write/read speeds, a dense circuit integration, and accelerated data processing.[3,4] However, one of the fundamental characteristics of spintronic materials is their ability to enhance spin polarizability up to a certain temperature limit.[5] Consequently, these compounds have potential applications in industrial spin filters, spin valves, magnetic memories, and magnetic sensors, offering a broad range of applicability in the sensor industry.[6]

Nowadays, one of the most active components in spintronics is half-metallic ferromagnets (HMF), which belong to the class of spin-polarized materials.[7] These materials exhibit no band gap in one spin state while possessing a band gap in the other, demonstrating metallic behavior in one spin state and insulating or semiconducting behavior in the other.[8]

Half-metallic ferromagnetism was first discovered by de Groot and his colleagues in 1983 in PtMnSb and NiMnSb.[9] Numerous experimental and theoretical studies have demonstrated the performance of HMFs in various materials, including metal oxides like,[10,11] Heusler alloys,[12,13] simple perovskites and their alloys,[14–17] double perovskites[18–20] and doped compounds.[21–23] However, many of these materials suffer from significant drawbacks that limit their practical applications, including low magnetic ordering temperatures, complex synthesis processes, and the degradation of half-metallic responses due to spin-flip transitions. Although substantial efforts have been made, achieving 100% spin polarization at room temperature remains a challenging task.[24]

Recently, K_2PtCl_6-type cubic variant perovskite inorganic compounds have garnered significant attention due to their favorable half-metallic properties and 100% spin polarizability.[25–29] Among this group, X_2TaCl_6 (X = K, Cs) remains largely unexplored in terms of its complete physical properties relevant to spintronic applications. Existing literature predominantly discusses their lattice parameters, bulk modulus, and other structural characteristics. Brik *et al.*[30] established an empirical relationship between lattice constants, ionic radii, and electronegativity of the K/Cs, Ta, and Cl ions, calculating the lattice constant of K_2TaCl_6 to be 9.9935 Å and

[a]*Department of Physics, Government Post Graduate Jahanzeb College Saidu Sharif, Swat 19130, Khyber Pakhtunkhwa, Pakistan. E-mail: azmatupesh@gmail.com*
[b]*Department of Physics, College of Science, Umm Al-Qura University, Makkah 21955, Saudi Arabia*

that of Cs_2TaCl_6 to be 10.271 Å. Ali *et al.*[31] calculated the bulk modulus of K_2TaCl_6 and Cs_2TaCl_6 using a semi-empirical formula, resulting in bulk moduli of 36.38 GPa for K_2TaCl_6 and 33.12 GPa for Cs_2TaCl_6.

The literature review revealed a lack of complete physical properties for X_2TaCl_6 (X = K, Cs) variant perovskites. To address this gap, we employed spin-resolved density functional theory to determine the structural, magnetic, and electronic properties of these materials. This comprehensive study offers valuable insights into the physical properties of X_2TaCl_6, potentially paving the way for their use in spintronics based applications.

2 Calculations methodology

Preparation of materials for experimental applications is often time-consuming and energy-intensive. Therefore, density functional theory (DFT)[32] can be utilized to predict the accurate properties of materials prior to experiments, saving both time and resources. These calculations reliably align with experimental results and are widely accepted by researchers. In this rapidly advancing technological era, first-principles calculations offer a swift approach to identifying promising materials with minimal experimental effort. Therefore, to investigate the two variants of perovskites X_2TaCl_6, where X = K, Cs, we employed the full-potential linearized augmented plane wave (FP-LAPW) method DFT, as implemented in the Wien2k computational package.[33] The exchange–correlation potential was treated using the Perdew–Burke–Ernzerhof generalized gradient approximation (PBE-GGA).[34] To accurately account for the partially filled Ta d-states, an effective Hubbard on-site Coulomb parameter (U_{eff}) was introduced, following Duradev's approach,[35] which considers the difference between the Coulomb interaction U and the exchange parameter J. A U_{eff} value of 2.0 eV was adopted from the AFLOW library.[36] Charge convergence criteria were set to 0.001e, and atomic positions, cell size, and shape were optimized until the total energy converged within 0.0001 Ry. For detailed structural, density of states, and band structure calculations, a dense k-point mesh of 1000 points was used. The optimized anion structural parameters (X) were found to be 0.243 for and 0.244 for K_2TaCl_6 and Cs_2TaCl_6, respectively. Additionally, the phonon dispersion curves have been calculated using CASTEP code of DFT.[37]

3 Results and discussion

3.1 Confirmation of stability

X_2TaCl_6 (X = K, Cs) compounds (shown in Fig. 1) belong to space group *Fm3m* and crystallize in K_2PtCl_6 type structure, with four formula units in one-unit cell. Where, X, Ta and Cl atoms occupies (0.25, 0.25, 0.25), (0, 0, 0) and (X, 0, 0) position respectively. To confirm cubic phase stability of these compounds, we calculated tolerance factor (t) through below relation[38]

$$t = \frac{R_{K/Cs} + R_{Cl}}{\sqrt{2}(R_{Ta} + r_{Cl})} \quad (1)$$

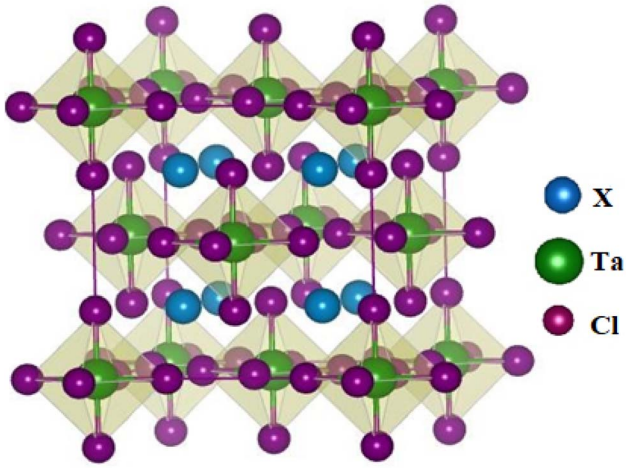

Fig. 1 Crystal structure of X_2TaCl_6 (X = K, Cs).

where, R_K (1.64), R_{Cs} (1.88), R_{Ta} (0.68) and R_{Cl} (1.81) are ionic radii of K, Cs, Ta and Cl in Å, respectively. The computed t for K_2TaCl_6 and Cs_2TaCl_6 is 0.98, 1.05, respectively. These values are within the allowed range of cubic phase;[39] therefore, confirm the cubic structure of both X_2TaCl_6 compounds.

To analyze ground state stability of studied X_2TaCl_6 compounds with respect to magnetism among NM (non-magnetic), FM (ferromagnetic) and AFM (anti ferromagnetisms), optimization process was adopted. Where, the volume of unit cell is varied in a range from −10 to 10% of experimental volume and the energy of each and every volume is noted. After that energies are plotted as function of volume as shown in Fig. 2. This figure makes it clear that both the studied compounds have minimum energy by considering their ground state as FM. Therefore, in proceeding sub sections we will consider X_2TaCl_6 compounds as FM.

On the way to confirm the thermodynamic stability in FM phase, the enthalpy of formation for X_2TaCl_6 compounds were calculated through below relation[40]

$$\Delta H_f = E_{tot}(X_2TaCl_6) - 2E_X - E_{Ta} - 6E_{Cl} \quad (2)$$

Here E_{tot} is the optimized ground state energy of X_2TaCl_6 compounds and E_X, E_{Ta}, and E_{Cl} are energies of constituent atoms in these compounds. The computed ΔH_f are −30.11428 eV for K_2TaCl_6 and −29.13729 eV for Cs_2TaCl_6. Negative sign in these energies confirms the thermodynamic stabilities of the compounds in FM phase. In addition, the negative sign indicates that formation reaction for K_2TaCl_6/Cs_2TaCl_6 is exothermic.

To assess the dynamical stability of the studied variant perovskites, phonon dispersion curves were computed and are shown in Fig. 3. With nine atoms per formula unit, there are twenty-seven phonons vibrational modes at each q-point, including three acoustic modes and twenty-four optical modes. The optical phonons exhibit a gap due to the heavier masses of the X and Ta atoms. The absence of any negative phonons frequencies confirms that both variant perovskites are dynamically stable.[41]

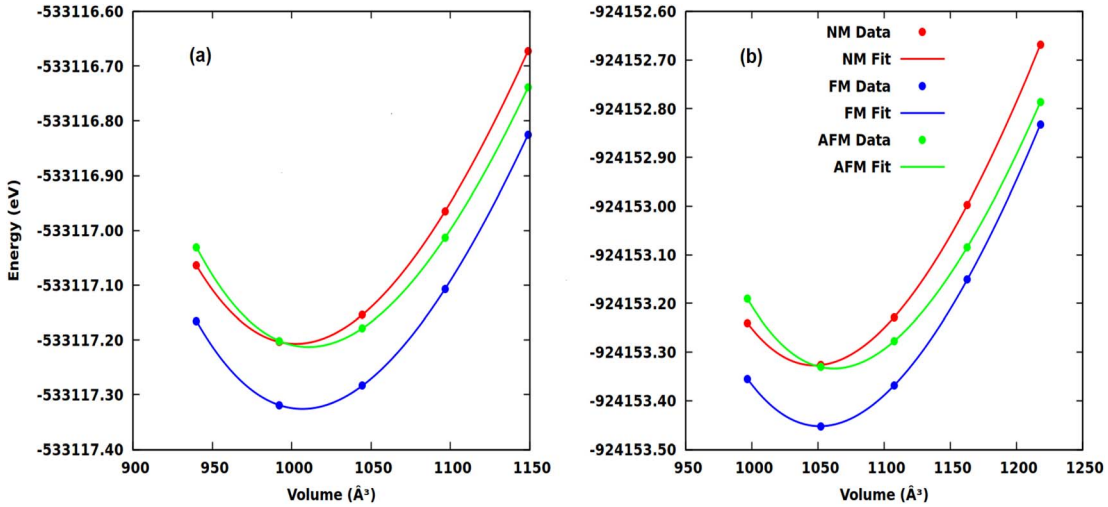

Fig. 2 Volume optimization plots of (a) K_2TaCl_6 and (b) Cs_2TaCl_6 in nonmagnetic (NM), ferromagnetic (FM) and anti-ferromagnetisms (AFM) phases with their corresponding fit by Birch–Murnaghan's equation of state.

One of the essential requirements for a compound to be used in a device fabrication, is its mechanical stability.[42–44] This stability for the studied perovskites was retrieved by calculating elastic constants C_{11}, C_{12}, and C_{44} (Table 1) through IRelast code.[45] These constants obey Born criteria of mechanical stability,[46] C_{11}, C_{12}, $C_{44} > 0$, $C_{11} - C_{12} > 0$, $C_{11} + 2C_{12} > 0$, and $C_{12} < B < C_{11}$. Therefore, X_2TaCl_6 variant perovskites are mechanically stable.

3.2 Structural parameters

The lattice constants of the investigated X_2TaCl_6 compounds were calculated using an analytical formula[47] that relates them to the ionic radii of the constituent ions:

$$a = xR_{K/Cs} + yR_{Ta} + zR_{Cl} \quad (3)$$

In this equation, the constants x, y, and z are 2.45322, 0.71042, and 2.92971, respectively.[47] $R_{K/Cs}$, R_{Ta} and R_{Cl} denote the ionic radii of K/Cs, Ta, and Cl ions, respectively. Additional structural parameters were obtained by fitting the data of volume optimization process into the Murnaghan equation of state[48] as shown in Fig. 2.

$$E(V) = E_o + \frac{19}{6}BV_o + \left[\left\{\left(\frac{V_o}{V}\right)^{2/3} - 1\right\}^3 B_P + \left\{\left(\frac{V_o}{V}\right)^{2/3} - 1\right\}^2 \left\{6 - 4\left(\frac{V_o}{V}\right)^{2/3}\right\}\right] \quad (4)$$

This fitting process allows the extraction of relevant structural details like bulk modulus (B), volume (V_o), lattice constant (a_o), pressure derivative of the bulk modulus (B_P), and the energy of ground state (E_o). Table 1 contain these details for X_2TaCl_6 perovskites only in stability phase (FM). Where, the lattice constant and volume of both compounds increase by replacing K with Cs, while the bulk modulus decreases. This trend is attributed to the larger ionic size of Cs compared to K.

Table 1 Calculated lattice constant (a_o), bulk modulus (B), variation of bulk modulus with pressure (B_P), volume (V_o), ground state energy (E_o), elastic constants (C_{11}, C_{12}, C_{44}) for X_2TaCl_6 (X = K, Cs) variant perovskites

	K_2TaCl_6		Cs_2TaCl_6	
Parameter	Present	Others	Present	Others
a_o (Å)	9.809[a]	9.921 (ref. 30)	10.3979[a]	10.398 (ref. 30)
	10.0258[b]	9.9935 (ref. 30)	10.1729[b]	10.271 (ref. 30)
V_o (Å^3)	1006.5174		1052.7720	
E_o (eV)	−533117.326		−924153.452	
B (GPa)	41.0209		40.7210	
B_P	4.5158		4.2674	
C_{11} (GPa)	85.407		80.113	
C_{12} (GPa)	22.088		25.546	
C_{44} (GPa)	17.325		22.871	

[a] Analytical. [b] Murnaghan equation of state.

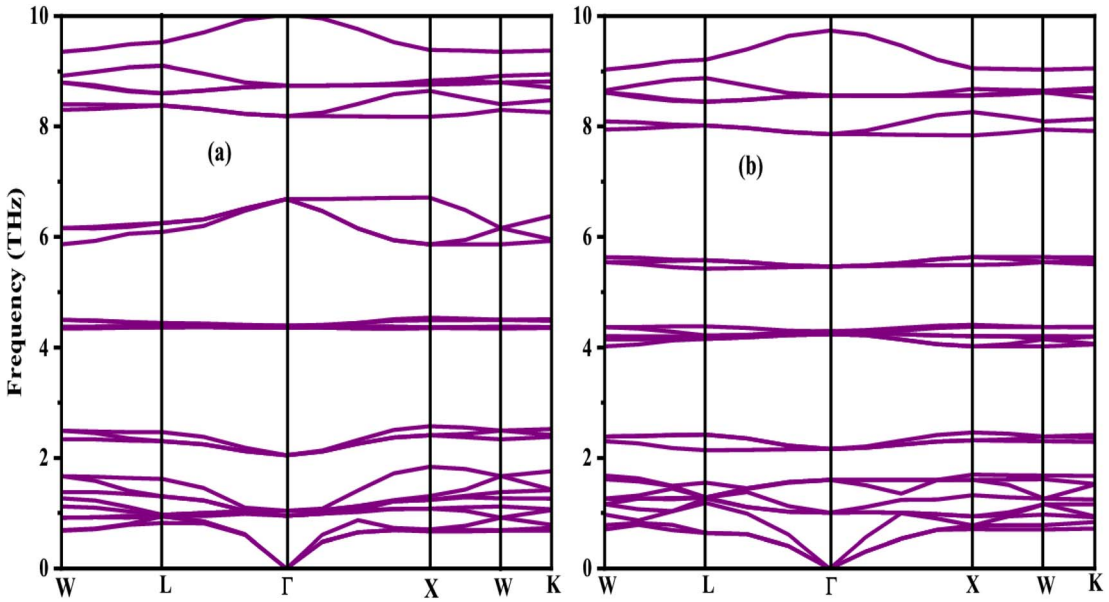

Fig. 3 Calculated phonon dispersion curve for (a) K_2TaCl_6 and (b) Cs_2TaCl_6 variant perovskites.

3.3 Electron density

The analysis of the electron density along the (110) plane, as visualized in Fig. 4 *via* Xcrysden, provides valuable insights into the bonding characteristics within the X_2TaCl_6 (X = K, Cs) variant perovskites. The prominent charge distribution observed between Ta and the halogen atom (Cl) indicates significant covalent interactions. In contrast, the spherical contour around the X atom signifies a predominantly ionic bonding character between X and the halogen atoms. The localized electron density around X indicates minimal covalent sharing, consistent with an ionic interaction. Such bonding behavior aligns with previous reports in similar perovskite structures,[49,50] reaffirming the general trend of covalent Ta–Cl bonding and ionic X–Cl interactions in these materials.

3.4 Electronic properties

To investigate the electronic properties of X_2TaCl_6 perovskites, spin-dependent total density of states (TDOS) calculations was performed using both GGA and GGA+*U* approaches, as depicted in Fig. 5. The results indicate that the total DOS profiles of both compounds exhibit similar characteristics. In spin-up channel, the Fermi level is fully occupied by electronic states, suggesting metallic behavior. Conversely, in the spin-down channel, the Fermi level remains unoccupied and resides with a band gap separating the valence and conduction bands. Consequently, both X_2TaCl_6 compounds function as semiconductors in the spin-down channel. This distinct spin-dependent electronic structure gives rise to spin polarization at the Fermi level, with the percentage of spin polarization calculable *via* the following relation:[51]

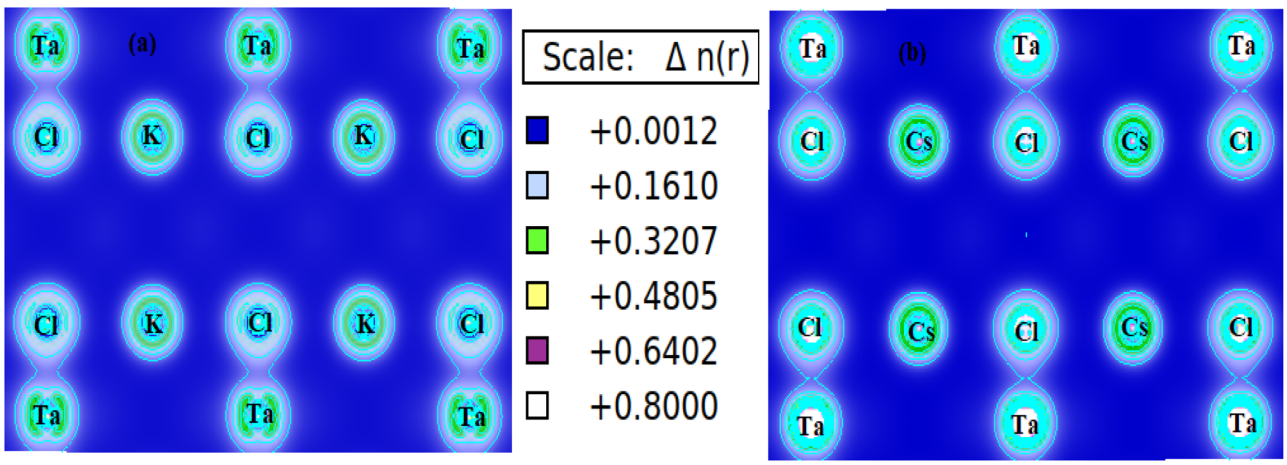

Fig. 4 Electron density plots for (a) K_2TaCl_6 and (b) Cs_2TaCl_6 variant perovskites.

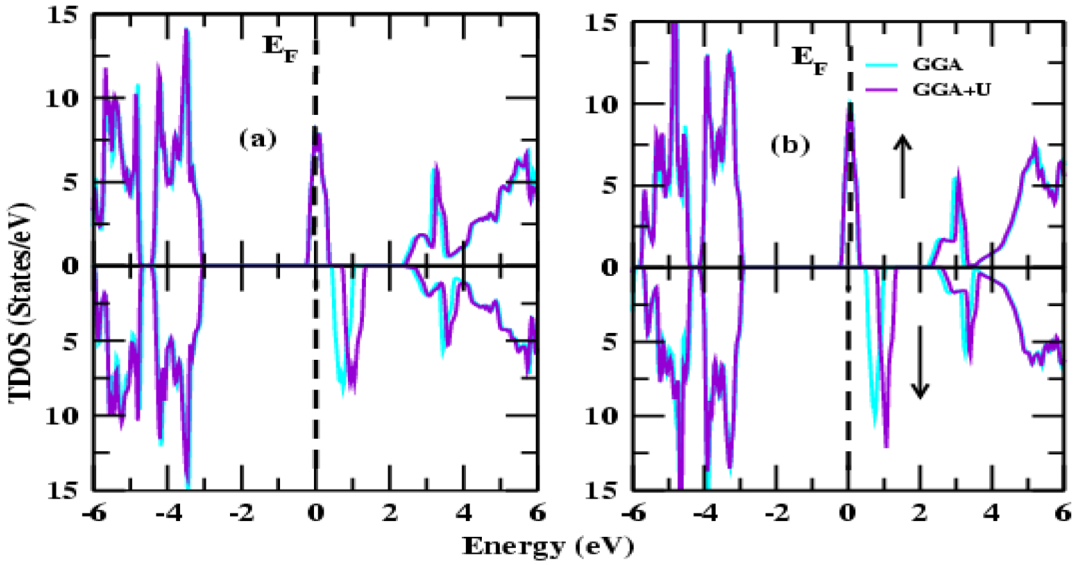

Fig. 5 Total density of states (DOS) of (a) K_2TaCl_6 and (b) Cs_2TaCl_6 variant perovskites.

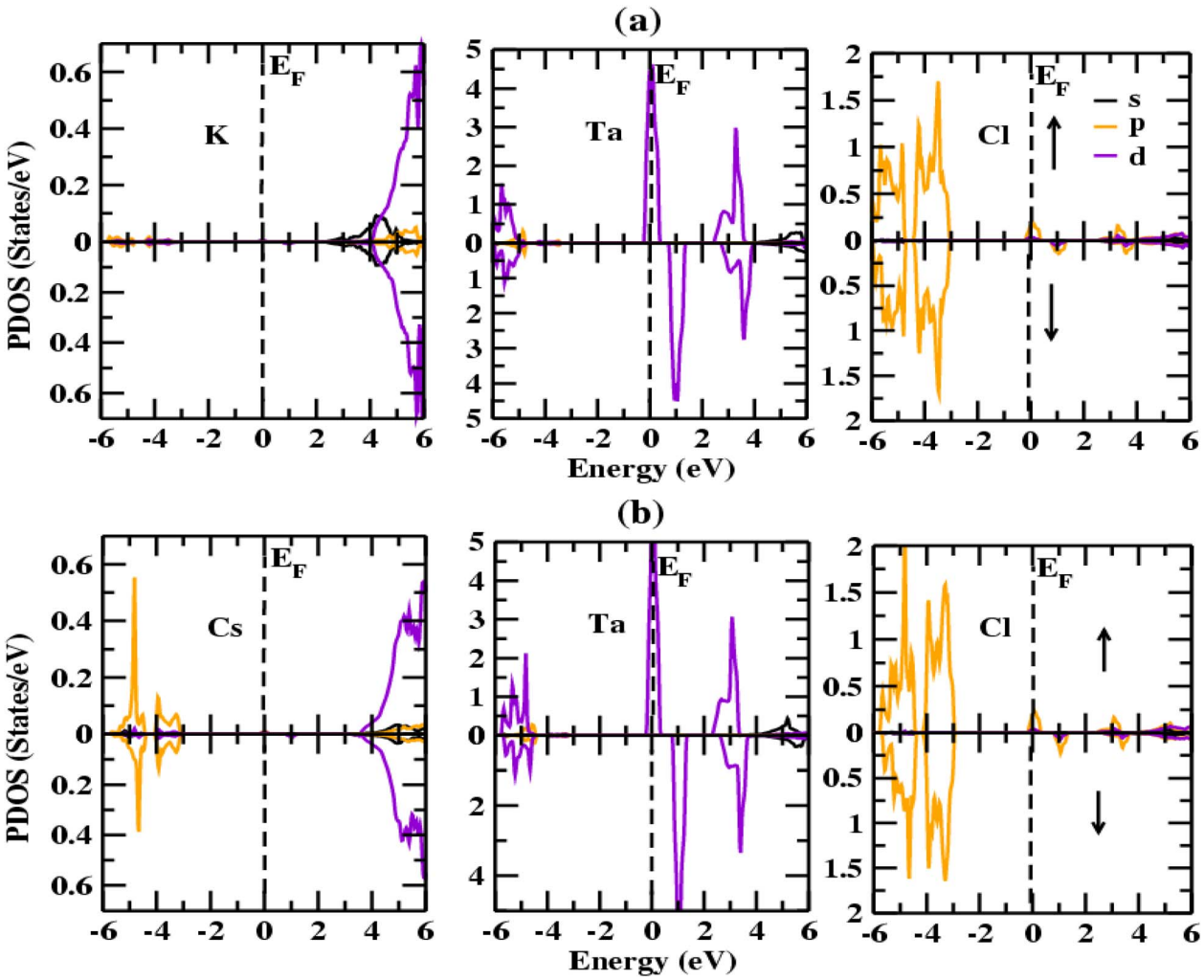

Fig. 6 Partial density of states (PDOS) of (a) K_2TaCl_6 and (b) Cs_2TaCl_6 variant perovskites.

$$P = \frac{N(\uparrow) - N(\downarrow)}{N(\uparrow) + N(\downarrow)} \times 100\% \quad (5)$$

where, $N(\downarrow)$ and $N(\uparrow)$ symbolize the TDOS at Fermi level in spin-down and in spin-up channels, respectively. The eqn (5) results 100% polarizability at the Fermi level. This maximum value of P gives guarantees of the use of these compounds for in spintronics based applications.

To gain a deeper understanding of the electronic structure of X_2TaCl_6 compounds based on the atomic orbitals of its constituent elements, the spin-polarized partial density of states (PDOS) was calculated and displayed in Fig. 6. This analysis highlights three distinct energy regions. The first region, spanning from −6 eV to −4 eV, is mainly composed of Cl-p states, with minor contributions from K/Cs-p and Ta-d orbitals in both spin channels. The second region, between −2 eV and 2 eV, contains states that are crucial to the material's half-metallic behavior. In the spin-up channel, Ta-d states cross the Fermi level, indicating metallic behavior. In contrast, in the spin-down channel, these states shift into the conduction band, leaving the Fermi level unoccupied and causing the material to exhibit semiconducting properties. Overall, the Ta-d orbitals play a key role in the observed half-metallicity. The third region, from 2 eV to 6 eV, is dominated by X-d and Ta-d states in both spin channels.

The spin-resolved electronic band structures of X_2TaCl_6 compounds were calculated along high-symmetry directions within the first Brillouin zone. It is well known that conventional DFT methods using GGA and LDA often underestimate the electronic properties of magnetic materials. To improve accuracy, additional band structure calculations were performed using GGA+U, with the results shown in Fig. 7. In the spin-up channel, the electronic states overlap at the Fermi level, indicating metallic behavior for X_2TaCl_6. In contrast, the spin-down channel exhibits both the valence band maximum and the conduction band minimum at the Γ point, confirming that these materials are direct band gap semiconductors. The computed band gaps for K_2TaCl_6 are 3.37 eV with GGA and 3.93 eV with GGA+U, while for Cs_2TaCl_6, the gaps are 3.34 eV with GGA and 3.62 eV with GGA+U.

3.5 Magnetic properties

Magnetic properties are fundamental for determining a material's applicability in spintronics. In a compound, magnetism primarily arises through either double exchange or super-exchange interactions among magnetic cations and non-magnetic anions. Double exchange promotes ferromagnetism, whereas super-exchange typically results in antiferromagnetic ordering.[52] Super-exchange involves an indirect coupling between neighboring cations mediated by non-magnetic anions, where the d-orbitals of both atoms contain electrons with either identical localization or differing by two electrons.[53] In contrast, double exchange is a magnetic interaction characterized by the transfer of an electron between two atoms while maintaining its spin orientation.[53] In our study, the most stable energy configuration identified during optimization indicates the presence of ferromagnetism in K_2TaCl_6 and Cs_2TaCl_6.

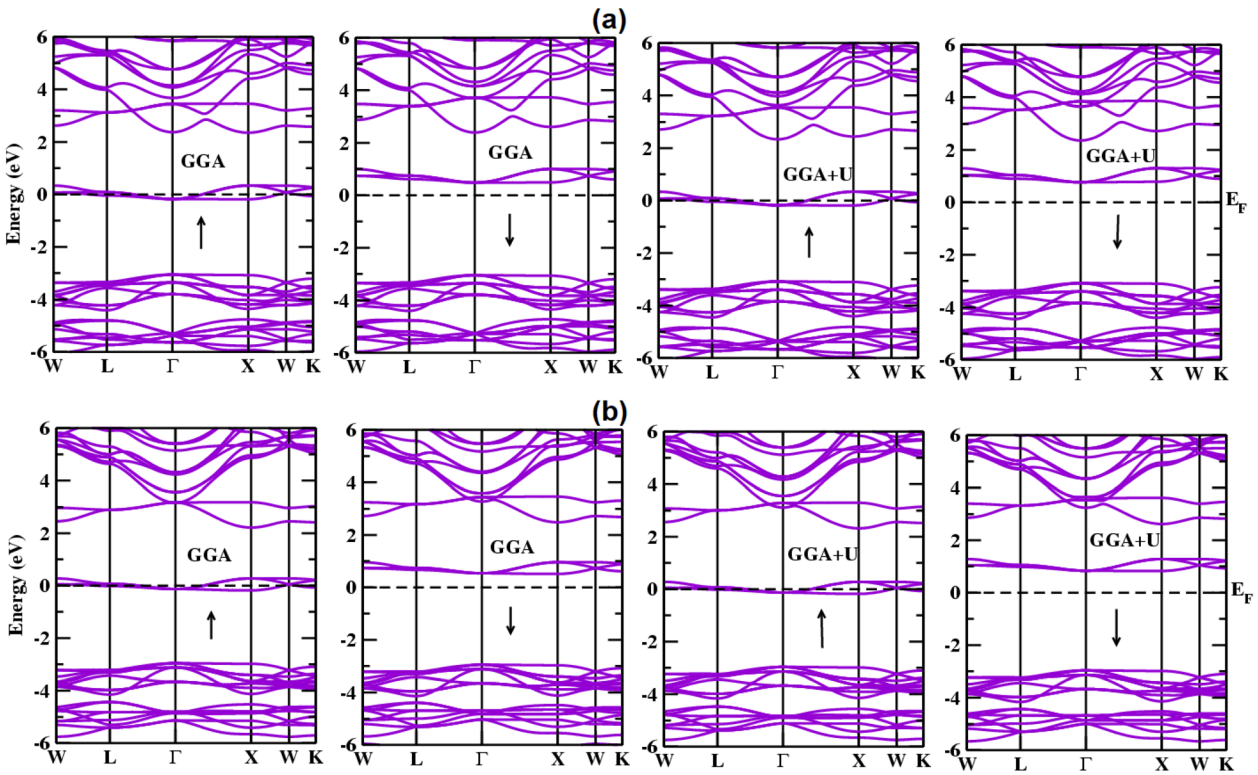

Fig. 7 Band structures of (a) K_2TaCl_6 and (b) Cs_2TaCl_6 variant perovskites.

Table 2 Calculated interstitial region (M_{int}), atomic ($M_{K/Cs}$, M_{Ta} and M_{Cl}) and total (M_{tot}) magnetic moments (in μ_B) of K_2TaCl_6 and Cs_2TaCl_6 variant perovskites

Compound	Method	M_{int}	$M_{K/Cs}$	M_{Ta}	M_{Cl}	M_{tot}
K_2TaCl_6	GGA	0.27544	0.00131	0.70216	0.00330	1.00
	GGA+U	0.27904	0.00122	0.72730	−0.00146	1.00
Cs_2TaCl_6	GGA	0.25933	0.00120	0.72706	0.00188	1.00
	GGA+U	0.26353	0.00093	0.75664	−0.00365	1.00

Consequently, the ferromagnetic behavior in X_2TaCl_6 compounds originates from double exchange interactions between Ta cations and Cl anions. Table 2 summarizes the magnetic moments within the interstitial regions, on individual atoms, and across the entire unit cell. The dominant contribution to the total magnetic moment arises from Ta atoms, while contributions from K or Cs and Cl atoms are minimal. Additionally, as reported in previous studies,[54,55] these compounds exhibit half-metallic ferromagnetism, characterized by a total magnetic moment (M_{tot}) expressed as an integer value. The calculated M_{tot} for both X_2TaCl_6 compounds is $1\mu_B$, consistent with the criteria for half-metallicity.

To insight more deeply into the magnetic behavior, the phenomenon of crystal field splitting in Fig. 8 has been considered for octahedral coordination environment of X_2TaCl_6 variant perovskites. Where, in the neighborhood of the Fermi level, Cl atoms split Ta-d states into two sets: the lower energy t_{2g} orbitals (d_{xy}, d_{yz} and d_{zx}) and high energy e_g orbitals ($d_{x^2-y^2}$ and d_{z^2}).[42,56] The single unpaired d electron occupies t_{2g} orbitals and giving to spin only magnetic moment[57] ($\sqrt{n(n+2)}$) of $1.73\mu_B$, which higher than our calculated value. The apparent difference can be explained on the basis of PDOS in Fig. 9. Where, a strong hybridization between Ta–d-t_{2g} and Cl–p sates can be seen. As result, d^1 electron delocalizes and reduces the local moment relative to the purely ionic crystal field theory limit. This covalency-driven delocalization is well known in transition-metal halides[58]

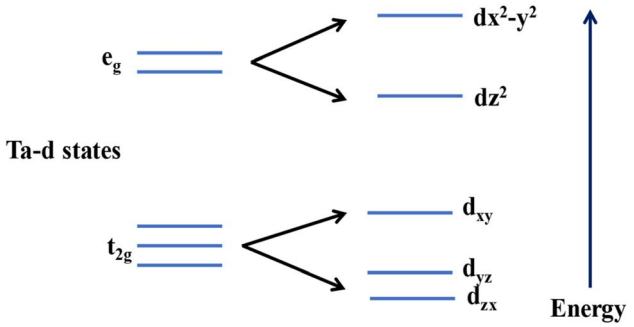

Fig. 8 Splitting of Ta-d states in X_2TaCl_6 (X = K, Cs) variant perovskites at octahedral site.

3.6 Curie temperature

In addition to exhibiting spin-polarized states at the Fermi level, a key requirement for spintronic applications is a high Curie temperature (T_C). Materials with T_C exceeding room temperature are essential for practical device implementation. In this work, the T_C values for X_2TaCl_6 compounds were estimated using the mean field approximation (MFA) based on classical Heisenberg model, expressed as $K_BT_C = 2\Delta E/3y$, where y represent the number magnetic atoms, K_B is the Boltzmann constant, ΔE equals to $E_{AFM} - E_{FM}$.[59,60] The MFA calculations yield T_C values ad 875.32 K for K_2TaCl_6 and 918.45 for Cs_2TaCl_6. To enhance the accuracy of these estimates, the results were refined using the random phase approximation (RPA), which is related with MFA predictions as $(T_C)_{MFA}/(T_C)_{RPA} = 3/2$.[61] Consequently, the RPA-derived T_C values are 583.55 K for K_2TaCl_6 and 612.30 for Cs_2TaCl_6. These high values indicate

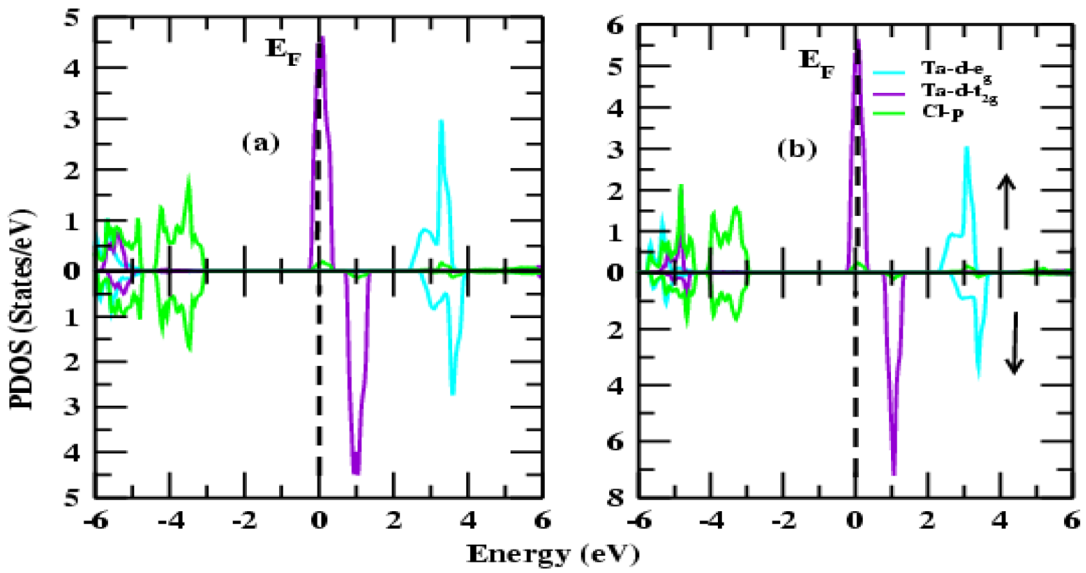

Fig. 9 Calculated crystal field splitting in (a) K_2TaCl_6 and (b) Cs_2TaCl_6 variant perovskites.

that X_2TaCl_6 compounds are highly promising candidates for spintronic device applications.

4 Conclusion

In this study, we have comprehensively investigated the structural, electronic, and magnetic properties of X_2TaCl_6 (X = K, Cs) compounds, which are cubic, perovskite-related inorganic materials analogous to K_2PtCl_6-type structures, using density functional theory calculations. Volume optimization confirmed ferromagnetic ground states for both compounds. The negative formation energies and positive phonon frequencies indicate their thermodynamic and dynamical stability in the cubic phase. The computed lattice parameters show excellent agreement with existing literature. Electronic structure analyses reveal that both compounds exhibit half-metallic behavior with complete spin polarization at the Fermi level. Each compound possesses a total magnetic moment of $1\mu_B$, arising from contributions of both the constituent atoms and the interstitial regions. The estimated Curie temperatures are sufficiently high to suggest potential stability at and above room temperature. Based on these findings, X_2TaCl_6 compounds emerge as promising candidates for spintronic applications.

Author contributions

MAA: investigation; visualization; calculations; writing original draft; methodology; conceptualization; review and editing, supervision, OA: calculations; software; investigation; review and editing; resources.

Conflicts of interest

The authors declare that they have no known competing financial interests or personal relationships that could have appeared to influence the work reported in this paper.

Data availability

The authors declare that the data supporting the findings of this study are available within the article.

References

1 R. Paudel, J.-C. Zhu, M. W. Qureshi, M. K. Hussain and D. Paudyal, *J. Magn. Magn. Mater.*, 2021, **539**, 168425.
2 M. Mebrek, A. Mokaddem, F. Bouasria, B. Doumi, A. Mir and A. Yakoubi, *Acta Phys. Pol. A*, 2019, **136**, 454–459.
3 R. Ullah, M. A. Ali, G. Murtaza, A. Khan and A. Mahmood, *Int. J. Energy Res.*, 2020, **44**, 9035–9049.
4 G. A. Prinz, *Science*, 1998, **282**, 1660–1663.
5 H. Rached, *Int. J. Quantum Chem.*, 2021, **121**, e26647.
6 M. Hariharan and R. D. Eithiraj, *J. Magn. Magn. Mater.*, 2024, **589**, 171553.
7 M. Berrahal, A. Bentouaf, H. Rached, R. Mebsout and B. Aissa, *Mater. Sci. Semicond. Process.*, 2021, **134**, 106047.
8 M. E. A. Monir, *Philos. Mag.*, 2020, **100**, 2524–2539.
9 R. D. Groot, F. Mueller, P. Van Engen and K. Buschow, *Phys. Rev. Lett.*, 1983, **50**, 2024–2027.
10 S. P. Lewis, P. B. Allen and T. Sasaki, *Phys. Rev. B: Condens. Matter Mater. Phys.*, 1997, **55**, 10253.
11 F. J. Jedema, A. Filip and B. Van Wees, *Nature*, 2001, **410**, 345–348.
12 Y. Al-Douri and M. Ameri, *Crit. Rev. Solid State Mater. Sci.*, 2025, **50**, 189–238.
13 K. Elphick, W. Frost, M. Samiepour, T. Kubota, K. Takanashi, H. Sukegawa, S. Mitani and W. Frost, *Sci. Technol. Adv. Mater.*, 2021, **22**, 235–271.
14 S. A. Khandy, I. Islam, D. C. Gupta, R. Khenata, A. Laref and S. Rubab, *Mater. Res. Express*, 2018, **5**, 105702.
15 S. A. Dar, S. A. Khandy, I. Islam, D. C. Gupta, U. K. Sakalle and V. Srivastava, *Chin. J. Phys.*, 2017, **55**, 1769–1779.
16 F. Nejadsattari, Z. M. Stadnik, Y. Nagata and T. Ohnishi, *Phys. B*, 2019, **553**, 59–67.
17 R. Soulen, J. Byers, M. Osofsky, B. Nadgorny, T. Ambrose and S. Cheng, *Science*, 1998, **282**, 85–88.
18 M. Ishfaq, A. R. Iftikhar, H. Ali, K. Ismail, G. Murtaza, G. A. A. M. Al-Hazmi and M. Jamil, *Mater. Sci. Eng. B*, 2025, **317**, 118198.
19 R. Masrour, G. Kadim, A. Jabar, E. K. Hlil and M. Ellouze, *Appl. Phys. A*, 2022, **128**, 1023.
20 K. I. Kobayashi, T. Kimura, H. Sawada, K. Terakura and Y. Tokura, *Nature*, 1998, **395**, 677–680.
21 Y.-H. Zhao, G.-P. Zhao, Y. Liu and B.-G. Liu, *Phys. Rev. B: Condens. Matter Mater. Phys.*, 2009, **80**, 224417.
22 X.-F. Ge and Y.-M. Zhang, *J. Magn. Magn. Mater.*, 2009, **321**, 198–202.
23 G. Rahman, S. Cho and S. C. Hong, *Phys. Status Solidi B*, 2007, **244**, 4435–4438.
24 Y. Bouldiab, S. Terkhi, Z. Aziz, F. Bendahma, M. A. Bennani, R. Bentata and M. A. Boudjeltia, *Int. J. Mod. Phys. B*, 2021, **35**, 2150202.
25 M. A. Ali, G. Murtaza, A. Khan, E. Algrafy, A. Mahmood and S. M. Ramay, *Int. J. Quantum Chem.*, 2020, **120**, e26357.
26 S. Khan, Z. Khan, M. A. Ali, T. A. Alrebdi, M. M. Saad H.-E. and N. U. Rahman, *J. Inorg. Organomet. Polym. Mater.*, 2025, **35**, 1259–1268.
27 H. A. Alburaih, S. Nazir, N. A. Noor, A. Laref and M. M. Saad H.-E., *RSC Adv.*, 2024, **14**, 1822–1832.
28 S. A. Khandy, I. Islam, B. Boussaida, R. Masrour, K. Kaur and Z. Gong, *J. Phys. Chem. C*, 2025, **129**, 5736–5746.
29 M. A. Yasir, G. M. Mustafa, M. A. Ameer, N. A. Noor, S. Mumtaz and I. M. Moussa, *Mater. Sci. Eng., B*, 2025, **311**, 117830.
30 M. G. Brik and I. Kityk, *J. Phys. Chem. Solids*, 2011, **72**, 1256–1260.
31 R. Ullah, M. A. Ali, G. Murtaza and A. H. Reshak, *Inorg. Chem. Commun.*, 2022, **129**, 109315.
32 P. Hohenberg and W. Kohn, *Phys. Rev.*, 1964, **136**, B864.
33 P. Blaha, K. Schwarz, P. Sorantin and S. B. Trickey, *Comput. Phys. Commun.*, 1990, **59**, 399.
34 J. P. Perdew, K. Burke and Y. Wang, *Phys. Rev. B: Condens. Matter Mater. Phys.*, 1996, **54**, 16533.

35 S. L. Duradev, G. A. Botton, S. Y. Savrasov, C. J. Humphreys and A. P. Sutton, *Phys. Rev. B: Condens. Matter Mater. Phys.*, 1998, **57**, 1505.
36 W. Setyawan, R. M. Gaume, S. Lam, S. R. Feigelson and S. Curtarolo, *ACS Comb. Sci.*, 2011, **13**, 382.
37 S. J. Clark, M. D. Segall, C. J. Pickard, P. J. Hasnip, M. J. Probert, K. Refson and M. C. Payne, *Z. Kristallogr.*, 2005, **220**, 567–570.
38 C. J. Bartel, C. Sutton, B. R. Goldsmith, R. Ouyang, C. B. Musgrave, L. M. Ghiringhelli and M. Scheffler, *Sci. Adv.*, 2019, **5**, eaav0693.
39 S. A. Dar and B. Want, *J. Phys. Chem. Solids*, 2023, **174**, 111135.
40 T. Tang, D. Hu, X. Zhao, L. Li and Y. Tang, *Phys. Scr.*, 2022, **97**, 125821.
41 G. Ding, C. Xie, J. Gong, J. Wang, J. Bai, W. Wang, D. Li, X.-P. Li and X. Wang, *Phys. Rev. B*, 2023, **108**, 075201.
42 Q. Gao, I. Opahle and H. Zhang, *Phys. Rev. Mater.*, 2019, **3**, 024410.
43 Q. Gao, T. Lin, W. Wang, G. Shi, X. Jin and C. Shen, *J. Mater. Chem. C*, 2025, **13**, 6375–6389.
44 Q. Gao, T. Liu, X. Jin, G. Shi and C. Shen, *J. Solid State. Chem.*, 2025, **341**, 125072.
45 M. Jamal, S. J. Asadabadi and I. Ahmad, *Comput. Mater. Sci.*, 2014, **95**, 592.
46 S. A. Dar, V. Srivastava and U. K. Sakalle, *J. Electron. Mater.*, 2017, **46**, 6870.
47 V. A. Sidey, *J. Phys. Chem. Solids*, 2019, **126**, 310–313.
48 F. Murnaghan, *Proc. Natl. Acad. Sci. U. S. A.*, 1944, **30**, 244.
49 T. Ghrib, A. Rached, E. Algrafy, I. A. Al-nauim, H. Albalawi, M. G. B. Ashiq, B. U. Haq and Q. Mahmood, *Mater. Chem. Phys.*, 2021, **264**, 124435.
50 M. A. Ali, A. A. A. Bahajjaj, S. Al-Qaisi, M. Sillanpää, A. Khan and X. Wang, *J. Comput. Chem.*, 2023, **44**, 1875–1883.
51 M. K. Hussain, O. T. Hassan and A. M. Algubili, *J. Electron. Mater.*, 2018, **47**, 6221–6228.
52 S. Blundell, *Magnetism in Condensed Matter*, Oxford University Press, New York, NY, 2001.
53 C. Zener, *Phys. Rev.*, 1951, **82**, 403.
54 A. Abbad, H. A. Bentounes, W. Benstaali, S. Bentata and B. Bouadjemi, *Chalcogenide Lett.*, 2015, **12**, 301.
55 A. Abbad, W. Benstaali, H. A. Bentounes, S. Bentata and Y. Benmalem, *Solid State Commun.*, 2016, **228**, 36.
56 Q. Gao, H.-H. Xie, L. Li, G. Lei, J.-B. Deng and X.-Ru Hu, *Superlattices Microstruct.*, 2015, **85**, 536–542.
57 D. C. Binwal, P. P. Mudoi, D. P. Panda and P. Vishnoi, *RSC Adv.*, 2023, **14**, 3982.
58 J. Kanamori, *J. Phys. Chem. Solids*, 1959, **10**, 87–98.
59 X. Wei, Y. Chu, X. Sun and J. Deng, *Eur. Phys. J. B*, 2013, **86**, 450.
60 P. Kurz, G. Bihlmayer and S. Blugel, *J. Phys. Condens. Matter*, 2002, **14**, 6353.
61 A. M. Kosevich, B. A. Ivanov and A. S. Kovalev, *Phys. Rep.*, 1990, **194**, 117–238.